

## Excitation functions of evaporation residues in heavy-ion reactions leading to compound nuclei with $Z = 80-90$

Sh. A. Kalandarov<sup>1,\*</sup>, G. G. Adamian<sup>1</sup>, and N. V. Antonenko<sup>1,2</sup>

<sup>1</sup>Joint Institute for Nuclear Research, 141980 Dubna, Russia

<sup>2</sup>Tomsk Polytechnic University, 634050 Tomsk, Russia

 (Received 14 June 2023; revised 6 October 2023; accepted 9 November 2023; published 29 November 2023)

The excitation functions of evaporation residues in  $xn$ ,  $pxn$ , and  $\alpha xn$  channels for the reactions leading to the compound nucleus with  $Z = 80-90$  are studied within the dinuclear system model. The stationary solution of master equation is applied to calculate the formation-decay probabilities of dinuclear systems. The results show that the maxima of excitation functions in  $xn$ ,  $pxn$ , and  $\alpha xn$  channels are comparable for the reactions leading to compound nuclei from Hg to Th. This means that the charged particles emission along with neutron emission influence the survival probability of compound nucleus in these reactions. Neutron deficiency of compound nucleus leads to favor both charged particle emission and fission.

DOI: [10.1103/PhysRevC.108.054612](https://doi.org/10.1103/PhysRevC.108.054612)

### I. INTRODUCTION

The studies of neutron-deficient and neutron-rich nuclei are required to define the borders of nuclear stability and to explore the shell evolution in isotopic chain. While the neutron-rich nuclei are produced in multineutron capture and transfer reactions, the neutron-deficient nuclei can be produced either in transfer reactions or in heavy-ion fusion reactions [1–7]. The compound nucleus (CN) formed in complete fusion of two nuclei is usually neutron deficient and could be highly rotating. The study of fusion of two heavy nuclei and the decay of the resulting excited CN is an actual topic of recent years. The practical interest of this research lies in synthesis of new neutron-deficient isotopes of heavy nuclei [1–6]. In the last decades, the nuclear chart was considerably extended with new isotopes and their properties were established [7].

The quasifission phenomena (the decay of the system without CN formation) was found to be the main obstacle to form the CN at small angular momentum  $J$  in the reactions with colliding nuclei having  $Z_1Z_2 > 1600$ . Such reactions with a large charge product  $Z_1Z_2$  are relevant to the synthesis of superheavy nuclei [2,8,9]. The quasifission also plays an important role in the reactions with  $Z_1Z_2 < 1600$  if the angular momentum is large because the repulsive centrifugal force becomes as strong as the Coulomb force. So in heavy-ion reactions there is always some competition between complete fusion and quasifission processes. The survival probability of formed CN depends on competition between particle evaporation and fission. For CN formed in particle-induced fission reactions, the main evaporation channel is neutron emission, which competes with fission process, while in heavy-ion reactions proton and  $\alpha$ -particle emission

from excited neutron-deficient CN become quite competitive decay channels. Accordingly, the determination of the fission barrier of such neutron-deficient and highly rotating hot nuclei becomes even more puzzling. These facts motivate us to investigate the excitation functions of evaporation residues in  $xn$ ,  $pxn$ , and  $\alpha xn$  decay channels in nuclear reactions leading to CN with  $Z = 80-90$  because this region of nuclei is mostly appropriate to investigate the role of neutron deficiency and rotation (angular momentum) on competition of particle emission channels with fission. The excitation functions for evaporation residues (ER) result from the consideration of this competition.

The ratio  $\Gamma_f/\Gamma_n$  of width for fission ( $\Gamma_f$ ) to one for neutron emission ( $\Gamma_n$ ) is an important and widely used characteristic of nuclear reactions related to fissility of CN. Using the experimental values of  $\Gamma_f/\Gamma_n$ , the fission barriers were extracted within the statistical model for CN with  $Z = 74-85$  [10]. This tool for extraction of fission barriers from experimental data is very useful when neutron emission and fission are dominant decay channels. However, for neutron-deficient and highly rotating CN formed in heavy-ion reactions, charged particle emission channels become quite strong and should be taken into account in the extraction of fission barriers from experimental  $\Gamma_f/\Gamma_n$ . Also, the experimental  $\Gamma_f$  may contain the contribution from quasifission process.

To calculate the excitation functions for ER in this paper, we apply the approach [11] based on the dinuclear system (DNS) model [12–15], which was successfully used for describing the decay process of excited medium mass CN. According to the DNS model, after projectile is captured by target, the nucleon exchange occurs between interacting nuclei. The nucleon exchange process drives the initial system to DNS with different mass and charge asymmetries. The CN is considered as a DNS with mass asymmetry  $\eta = 1$ . The decay of DNS in relative distance coordinate  $R$  and particle ( $n, p, \alpha$ ) evaporation from CN are in competition with

\*shuhrat@theor.jinr.ru

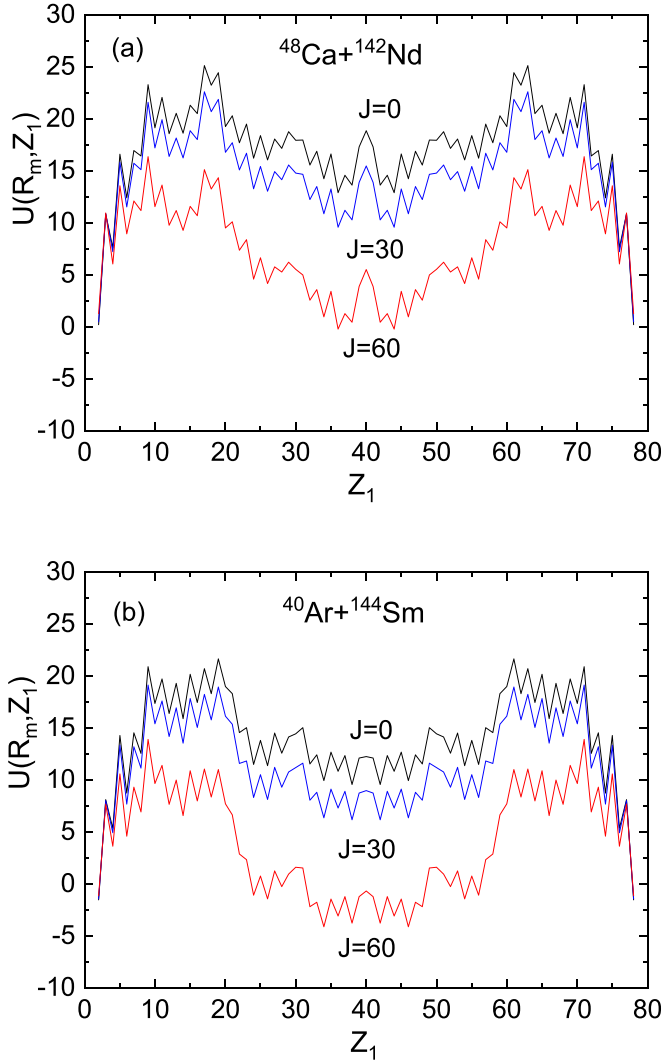


FIG. 1. Driving potentials  $U(R_m, Z_1, J)$  for the reactions (a)  $^{48}\text{Ca} + ^{142}\text{Nd}$  and (b)  $^{40}\text{Ar} + ^{144}\text{Sm}$  at indicated angular momenta  $J$ .

nucleon exchange process. The fusion-fission and quasifission products are formed as a result of decay of DNS in  $R$  and particle emission from CN leads to the formation of ER. Thus, our model describes the competition of all decay channels (from particle emission up to symmetric splitting) in a unique way. The excited CN can either emit particle or decay from one of the possible DNS configurations. Besides the description of deexcitation of excited CN, the DNS model is successful in the explanation of the properties of spontaneous fission [16]. In this approach to fission, the probability of each configuration is calculated as in the scission-point model [17]. Indeed, the widths of fission and particle emissions are calculated using the potential energies of prescission configurations.

The paper is organized as follows. In Sec. II, we present the most salient details of our model. In Sec. III, the comparison of calculated results with experimental data is discussed. The main conclusions are made in Sec. IV.

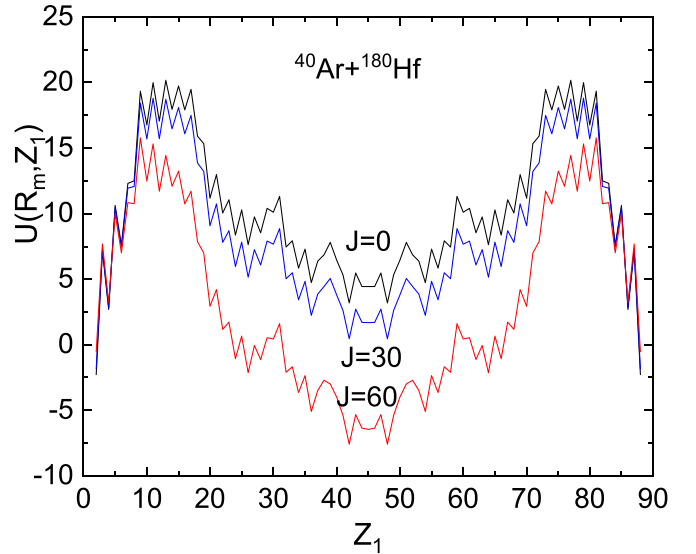


FIG. 2. Driving potential for the reaction  $^{40}\text{Ar} + ^{180}\text{Hf}$  at indicated angular momenta  $J$ .

## II. MODEL

In our model, the binary decay of excited nuclear system involves the motions in charge and mass ( $\eta$ ) asymmetry coordinates of the DNS and the motion in the relative distance coordinate  $R$  between the centers of mass of the nuclei in DNS. The nucleon exchange between nuclei in DNS transforms the initial DNS into different asymmetric and symmetric DNS and the CN. Since the decay of DNS in  $R$  is a collective motion, it requires some time, so that system before decaying from certain DNS can walk through many DNS configurations including the CN configuration due to fast nucleon exchange between nuclei. When system reaches CN configuration, it can either emit light particles (fusion

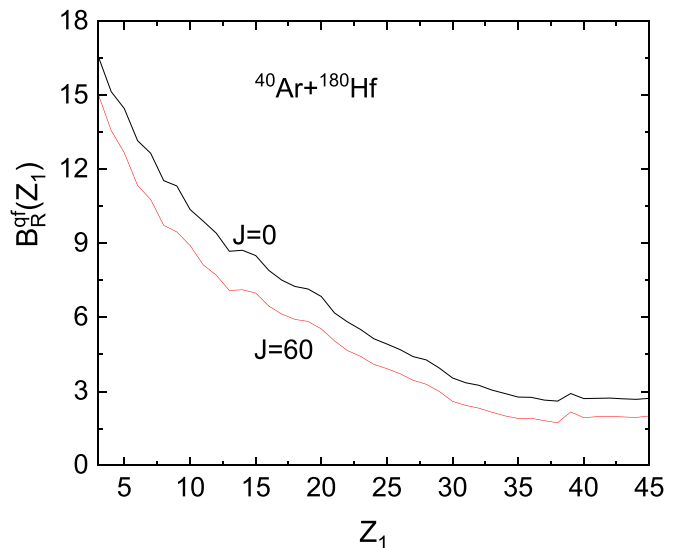


FIG. 3. Dependencies of quasifission barrier in DNS formed in the  $^{40}\text{Ar} + ^{180}\text{Hf}$  reaction on  $Z_1$  at indicated angular momenta  $J$ .

TABLE I. Calculated entrance Coulomb barrier  $V_b$ , excitation energy  $E_{\text{CN}}^*$  of CN for  $J = 0$  at  $E_{\text{c.m.}} = V_b$ , critical angular momentum  $J_{\text{cr}}$  and  $E_{\text{CN}}^*$  for  $J = 0$  at  $E_{\text{c.m.}}$  leading to  $J_{\text{max}} = J_{\text{cr}}$  for listed reactions. Energy units are given in MeV.

Reaction	$V_b$	$E_{\text{CN}}^*(E_{\text{c.m.}} = V_b, J = 0)$	$J_{\text{cr}}$	$E_{\text{CN}}^*$
$^{48}\text{Ca} + ^{142}\text{Nd} \rightarrow ^{190}\text{Hg}$	135.6	37	85	70
$^{40}\text{Ar} + ^{144}\text{Sm} \rightarrow ^{184}\text{Hg}$	128.5	37.5	83	75
$^{44}\text{Ca} + ^{156}\text{Gd} \rightarrow ^{200}\text{Po}$	144.5	46	80	78
$^{44}\text{Ca} + ^{160}\text{Gd} \rightarrow ^{204}\text{Po}$	143.8	50	83	85
$^{40}\text{Ar} + ^{166}\text{Er} \rightarrow ^{206}\text{Rn}$	137	46	73	72
$^{22}\text{Ne} + ^{190}\text{Os} \rightarrow ^{212}\text{Rn}$	86	48	66	88
$^{22}\text{Ne} + ^{194}\text{Pt} \rightarrow ^{216}\text{Ra}$	88.1	42	67	81
$^{22}\text{Ne} + ^{198}\text{Pt} \rightarrow ^{220}\text{Ra}$	87.7	40	68	80
$^{40}\text{Ar} + ^{180}\text{Hf} \rightarrow ^{220}\text{Th}$	144	43	76	74

evaporation) or go back to asymmetric DNS ( $\alpha$  particle + heavy nucleus) with further diffusion into more symmetric DNS then decaying in  $R$  (fusion fission). In this way, we describe the quasifission, fusion-evaporation, and fusion-fission processes within the DNS approach. The nature of these three modes of statistical decay are the same, the connections between them are provided by the mass asymmetry coordinate, only their characteristic times are different, the fusion-fission process is slower than the rest processes. This difference becomes more perceptible if decay time of the DNS becomes comparable to nucleon exchange time, which is typical for very heavy systems or for high angular momenta. The excited fragments of binary decays can also experience decay in the same way until the cold products are formed to be detected.

The nucleon exchange between the nuclei in DNS and its decay in  $R$  are usually described using transport approach with the master equation [18]. If the quasifission barriers  $B_R^{qf}$ , which prevent the DNS decay, are large enough, then one can use the stationary solution of this master equation to obtain the probability of finding the system in a given DNS,

which is proportional to relevant level density  $\rho$ . Thus, we assume that a statistical equilibrium is reached in mass-asymmetry coordinate so that the formation-decay probability  $W_{Z_1, A_1}$  with given asymmetries  $Z_1$  and  $A_1$  of each DNS or CN configuration depends on the corresponding potential energy

$$U(R, Z_1, A_1, J) = B_1 + B_2 + V(R, Z_1, A_1, J) - [B_{12} + V_{\text{CN}}^{\text{rot}}(J)], \quad (1)$$

calculated with respect to the potential energy  $B_{12} + V_{\text{CN}}^{\text{rot}}(J)$  [ $B_{12}$  is the mass excess of the CN and the rotational energy  $V_{\text{CN}}^{\text{rot}}(J)$  of the CN] of the rotating CN,  $B_1$ , and  $B_2$  are the mass excesses of fragments in their ground states. The nucleus-nucleus interaction potential  $V$  contains the nuclear, Coulomb, and centrifugal potentials. The orientations of the DNS nuclei correspond to the minimum of the potential energy (the pole-pole or tip-tip orientation for the deformed nuclei).

The formation-decay probability  $W_{Z_1, A_1}(E_{\text{c.m.}}, J)$  of the fragment  $(Z_1, A_1)$  is calculated as the product

$$W_{Z_1, A_1}(E_{\text{c.m.}}, J) = \frac{P_{Z_1, A_1} P_{Z_1, A_1}^R}{\sum_{Z'_1, A'_1} P_{Z'_1, A'_1} P_{Z'_1, A'_1}^R} \quad (2)$$

of the DNS formation probability  $P_{Z_1, A_1}$  and the DNS decay probability  $P_{Z_1, A_1}^R$ . In Eq. (2), the indexes  $Z'_1$  and  $A'_1$  go over all possible channels from the neutron evaporation to the symmetric DNS splitting. In the equilibrium limit in the charge and mass asymmetries (see Ref. [11] for details) the probability  $P_{Z_1, A_1}$  is calculated as follows:

$$P_{Z_1, A_1}(E_{\text{c.m.}}, J) \sim \exp[-U(R_m, Z_1, A_1, J)/T_{\text{max}}(J)]. \quad (3)$$

Here,  $n$ -,  $p$ -,  $d$ -, and  $t$ -evaporation channels are taken into consideration with  $U(R_m, Z_1, A_1, J) = 0$ . The DNS is formed at the touching distance  $R = R_m$  between the centers of nuclei. The value of  $R_m$  corresponds to a distance of about 0.5 fm larger than that corresponding to touching of nuclear

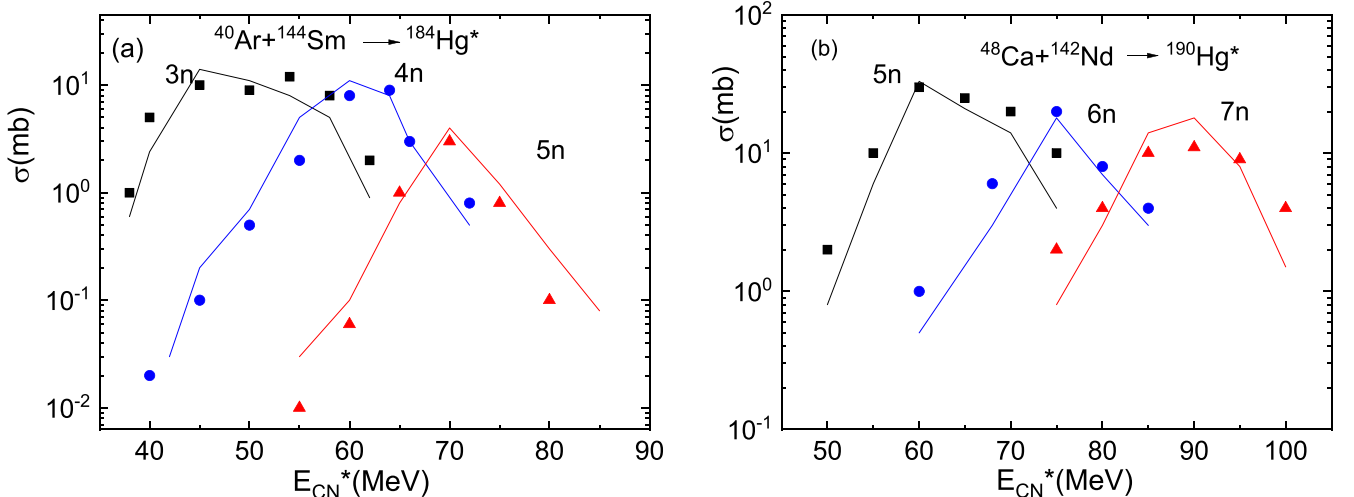


FIG. 4. Comparison of calculated (lines) and experimental (symbols) data for excitation functions in  $xn$  channels of the reactions (a)  $^{40}\text{Ar} + ^{144}\text{Sm}$  and (b)  $^{48}\text{Ca} + ^{142}\text{Nd}$ . The experimental data are taken from Ref. [19].

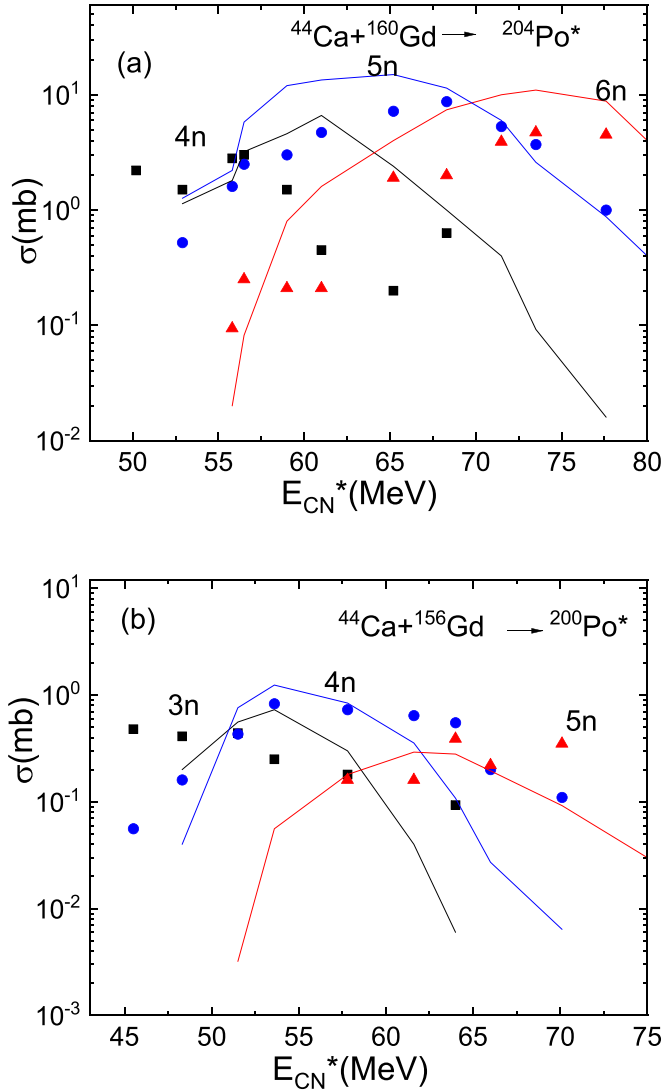


FIG. 5. Comparison of calculated (lines) and experimental (symbols) data for the excitation functions in  $xn$  channels of the reactions (a)  $^{44}\text{Ca} + ^{160}\text{Gd}$  and (b)  $^{44}\text{Ca} + ^{156}\text{Gd}$ . The experimental data are taken from Ref. [20].

surfaces [11]. The DNS decay probability

$$P_{Z_1, A_1}^R(E_{\text{c.m.}}, J) \sim \exp\left[-B_R^{qf}(Z_1, A, J)/T_{Z_1, A_1}(J)\right] \quad (4)$$

depends on  $B_R^{qf}(Z_1, A_1, J)$ , which is the difference between the potential energies of the DNS configurations at touching distance and at the barrier position. The quasifission barrier  $B_R^{qf}$  prevents the decay of the DNS in  $R$ . At  $J > J_{\text{cr}}$ ,  $B_R^{qf}(Z_1, A_1, J) = 0$  and  $P_{Z_1, A_1}^R = 1$ . In Eq. (3),  $T_{\text{max}}(J) = \max\{T_{Z_1, A_1}(J)\}$ , where  $T_{Z_1, A_1}(J)$  are the temperatures of the CN and all possible DNS with  $Z_1 \geq 2$ . For the emission of particles with  $Z_1 < 2$ ,  $T_{Z_1, A_1}(J) = T_{\text{CN}}(J)$  is the temperature of the CN and  $B_R^{qf}(Z_1, A_1, J)$  is equal to the particle binding energy plus the value of the corresponding Coulomb barrier at  $Z_1 \neq 0$ . Excitation energies of CN and DNS are

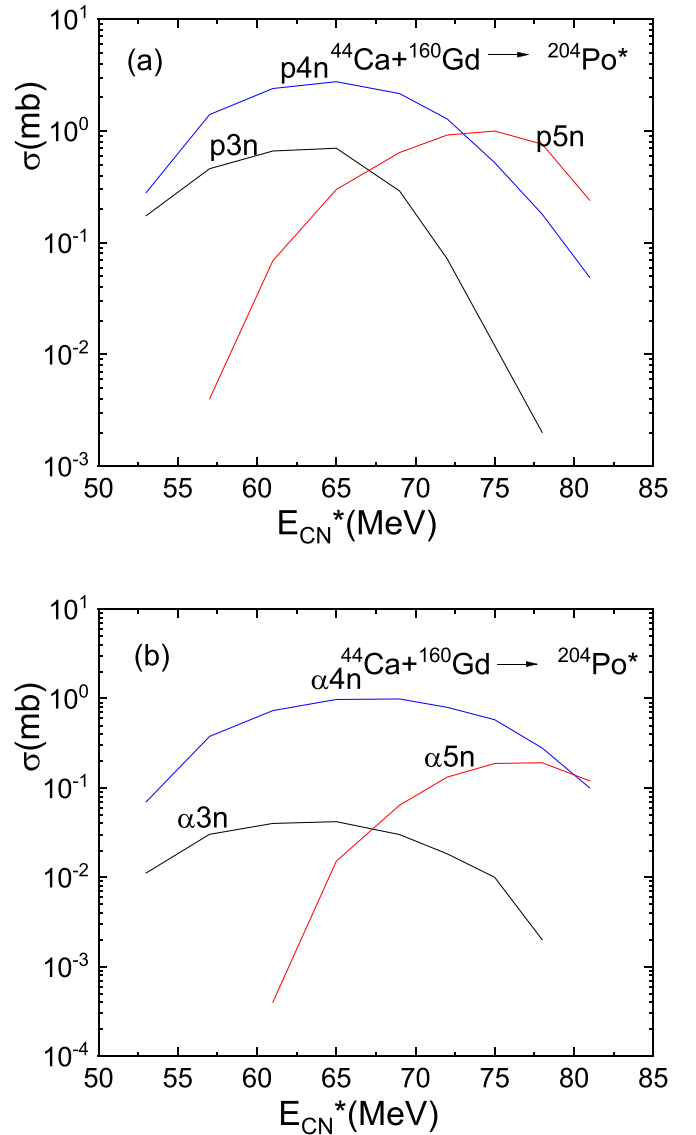


FIG. 6. Calculated excitation functions in (a)  $pxn$  and (b)  $\alpha xn$  evaporation channels of the  $^{44}\text{Ca} + ^{160}\text{Gd}$  reaction.

calculated as

$$E_{\text{CN}}^*(J) = E_{\text{c.m.}} + Q - V_{\text{CN}}^{\text{rot}}(J),$$

$$E_{\text{DNS}}^*(Z_1, A_1, J) = E_{\text{CN}}^*(J) - U(R_m, Z_1, A_1, J), \quad (5)$$

respectively. The local temperatures of CN and DNS are defined from their excitation energies using the Fermi-gas model formula  $T_{Z_1, A_1} = \sqrt{E_{\text{CN, DNS}}^*/a}$  with the asymptotic level-density parameter  $a = 0.114A + 0.162A^{2/3}$  [11]. Note that the number of neutrons emitted from the DNS (predecay neutrons) is very small in reactions considered [18].

In Eq. (2), the competition between various decay channels depends on the values of maximum angular momentum and excitation energy deposited in the system. Because theoretical descriptions of cluster decay and light-particle evaporation processes are related with the mass asymmetry coordinate, we use the same expressions (3) and (4) to calculate both processes. Fission and evaporation are the two obvious parts

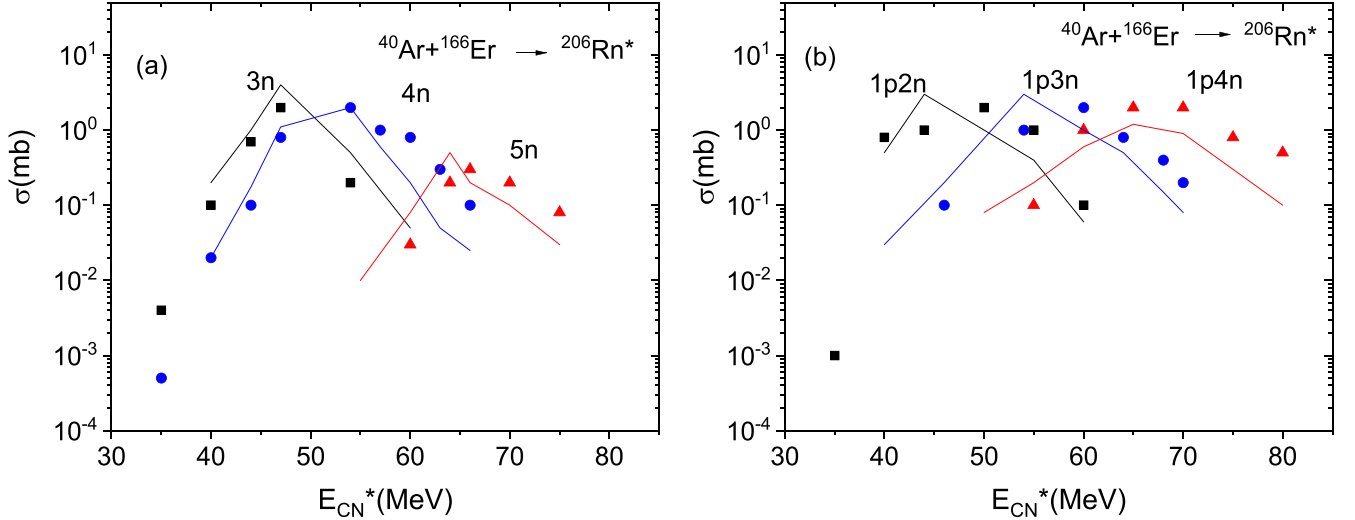


FIG. 7. Comparison of calculated (lines) and experimental (symbols) data for excitation functions in the (a)  $xn$  and (b)  $pxn$  evaporation channels of the  $^{40}\text{Ar} + ^{166}\text{Er} \rightarrow ^{206}\text{Rn}^*$  reaction. The experimental data are taken from Ref. [19].

of a single decay process. Note that the product  $P_{Z_1, A_1} P_{Z_1, A_1}^R$  in Eq. (2) takes into account the fusion-fission process together with the quasifission and fusion-evaporation processes. So, the binary decay fragments have contributions from both quasifission and fusion-fission, which can not be uniquely distinguished in our model.

Using the probabilities given in Eq. (2), we generate the cascade decay process of CN and DNS with the Monte Carlo technique. For this, we distribute all possible decay processes with the probabilities given in Eq. (2) in the interval  $[0; 1]$  and generate a random number to select the event. After each generation of the event, we redefine the mass and charge number, excitation energy, and angular momentum of the residual system and calculate new decay probabilities with Eq. (2). The generation of the events continues up to all decay fragments become deexcited. The evaporation particles are assumed to have Maxwellian kinetic energy distributions at given decay step. The excitation energy and angular momentum are divided between decay fragments according to their masses and moments of inertia, respectively. In this work, the simulation number  $n_{\text{sim}} = 10^6$  in Monte Carlo method is chosen to have enough high statistics for decay channels of interest.

If at the first step of Monte Carlo simulation the particle ( $n$ ,  $p$ ,  $\alpha$ ) emission is generated, it means CN is formed. System can either emit further particles or decay through doorway DNS configuration into binary fusion-fission products. At the second step, the Monte Carlo simulation based on Eq. (2) may result in either particle emission or DNS decay, which is related to fusion-fission in our model. The ER originates from the consequence of particle emissions. If at the first step the decay of some DNS is generated, then the quasifission or fusion-fission products are formed. So in our model the fusion-fission and quasifission are partly discriminated by the first step of Monte Carlo simulation of the cascade decay.

The partial cross sections for the ER is

$$\sigma_{Z,A}(J) = \pi \lambda^2 (2J + 1) P_{\text{cap}}(J) \frac{n_{Z,A}(J)}{n_{\text{sim}}}, \quad (6)$$

where  $n_{Z,A}(J)$  is number of a given evaporation residue in  $n_{\text{sim}}$  runs. The partial capture probability  $P_{\text{cap}}(J)$  is calculated with the Hill-Wheeler formula in the same way as in Ref. [11]. Then one can calculate the total cross section

$$\sigma(Z, A) = \sum_{J=0}^{J_{\text{max}}} \sigma_{Z,A}(J) \quad (7)$$

for the formation of ER. Here the maximum value of angular momentum  $J_{\text{max}}$  is limited by either the kinematical angular momentum  $J_{\text{kin}}$  or by critical angular momentum  $J_{\text{cr}}$ , depending on which one is smaller:  $J_{\text{max}} = \min(J_{\text{kin}}, J_{\text{cr}})$ . Here,  $J_{\text{cr}}$  is the angular momentum for which the pocket in the entrance interaction potential disappears (see more details in Ref. [11]).

### III. RESULTS AND DISCUSSION

#### A. Application of the model and outcomes

Since our intention is to reveal the competition of charged particles emission as well as neutron evaporation with fission process, we choose the reactions leading to  $Z_{\text{CN}} = 80-90$ , so that the fission is not strongly dominant channel as in heavier nuclei. In heavy-ion fusion reactions the formed CN is neutron deficient and highly rotating. The neutron deficiency leads to enhancement of the probability of proton and  $\alpha$  particle evaporation, while fission probability increases with angular momentum. These effects are included in our model through the calculation of potential energy  $U$  with the experimental binding energies and centrifugal forces [11].

In Fig. 1, the driving potentials  $[U(R_m, Z_1, A_1, J)]$  are minimized by  $A_1$  for given  $Z_1$  and normalized to the energy of rotating CN) for  $^{184}\text{Hg}$  and  $^{190}\text{Hg}$  nuclei to demonstrate the effects of neutron number and angular momentum. One can see that with increasing angular momentum  $J$  the potential energy of DNS decreases with respect to that of CN, so the formation probability of more symmetric DNS increases. For more neutron-deficient system  $^{184}\text{Hg}$ , the binding energy of neutron

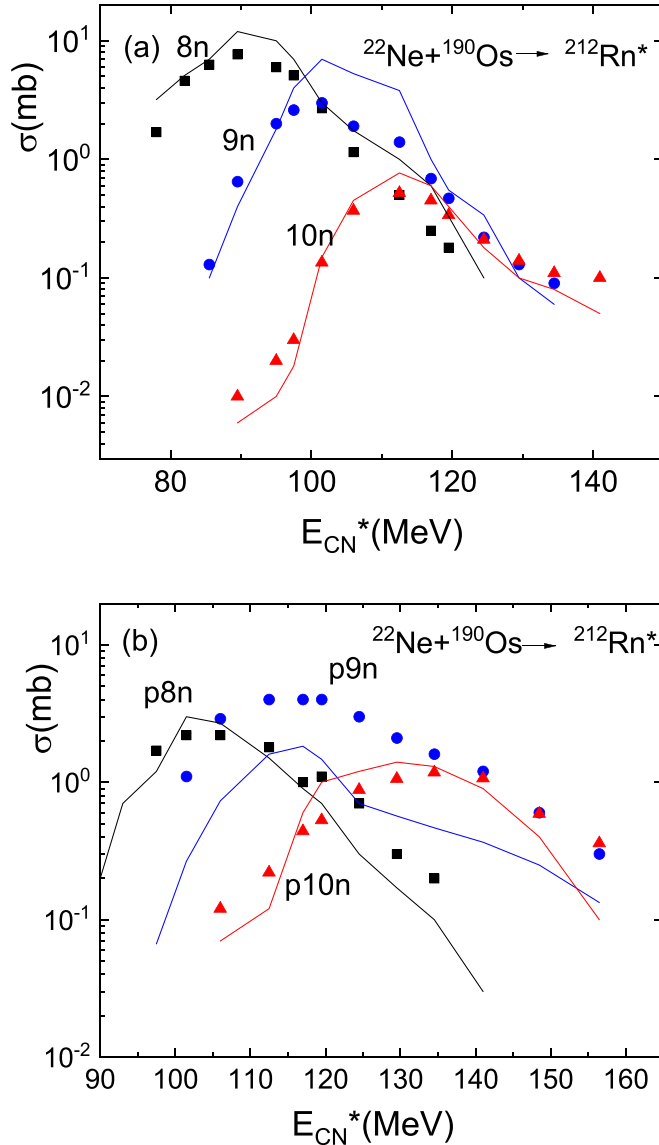


FIG. 8. Comparison of calculated (lines) and experimental (symbols) data for excitation functions in the (a)  $xn$  and (b)  $pxn$  evaporation channels of the reaction  $^{22}\text{Ne} + ^{190}\text{Os} \rightarrow ^{212}\text{Rn}^*$  reaction. The experimental data are taken from Ref. [21].

is larger and, as seen in Fig. 1, the formation of the DNS from the CN is energetically more favorable comparing to the system  $^{190}\text{Hg}$  with more neutrons. Since the separation energies of proton and  $\alpha$ -particle decrease with neutron deficiency, charged particle evaporation channels become competitive. In Fig. 2, the driving potential for heavier system  $^{220}\text{Th}$  is presented. One can see that symmetric DNS potential energy (about 5 MeV) becomes smaller than those for systems  $^{190}\text{Hg}$  (about 15 MeV) and  $^{184}\text{Hg}$  (about 10 MeV). This means that the formation probability of symmetric DNS increases, i.e., fissility of nuclei increases with  $Z_{CN}$ . The quasifission barrier  $B_R^{qf}(Z_1)$  in  $R$  as a function of  $Z_1$  at different angular momenta  $J$  is presented in Fig. 3 for  $^{220}\text{Th}$ . With increasing angular momentum from  $J = 0$  to  $J = 60$ , the value of  $B_R^{qf}(Z_1)$  is reduced to 1–1.5 MeV.

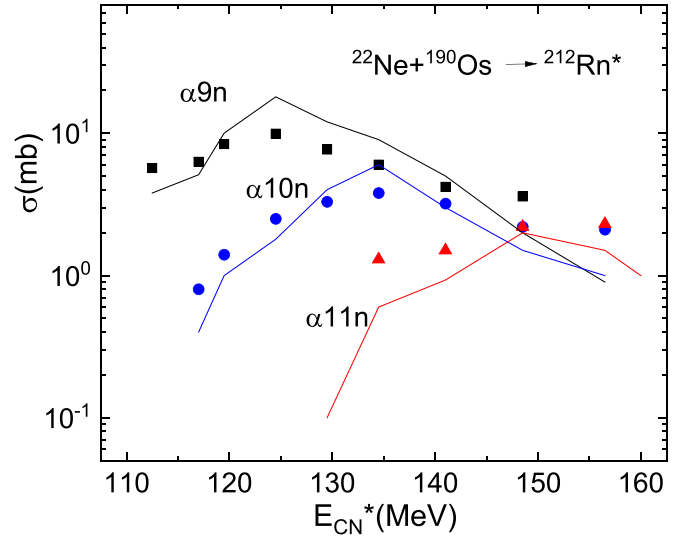


FIG. 9. Comparison of calculated (lines) and experimental (symbols) data for excitation functions in the  $\alpha xn$  channels of the  $^{22}\text{Ne} + ^{190}\text{Os} \rightarrow ^{212}\text{Rn}^*$  reaction. The experimental data are taken from Ref. [21].

We calculate excitation functions starting from slightly above Coulomb barrier energy  $V_b$ , which is calculated for spherical shapes of colliding nuclei. Maximal angular momentum  $J_{\max}$ , which contributes to capture process, increases by bombarding energy up to  $J_{\text{cr}}$ , for which capture probability is equal to zero. Further increasing of bombarding energy do not change  $J_{\max}$ , which remains to be  $J_{\max} = J_{\text{cr}}$ . The Coulomb barrier energies, the CN excitation energies corresponding to  $E_{\text{c.m.}} = V_b$ , critical angular momenta, the excitation energies of CN at which  $J_{\max}$  reaches  $J_{\text{cr}}$  are listed in Table I for the reactions considered.

Summary of the DNS model used in this work is as follows: (i) CN is considered as one of available very asymmetric DNS. If at the first step of Monte Carlo simulation the particle emission is generated, the CN formation is assumed. CN can further emit particles or go to fission through certain doorway DNS. (ii) Neutron deficiency, angular momentum and increasing charge number of CN lead to larger formation probability for symmetric DNS. (iii) The quasifission barrier  $B_R^{qf}$ , which prevents the DNS decay, increases with asymmetry and decreases with angular momentum. (iv) The maximal angular momentum  $J_{\max}$ , which contributes to capture process, is energy dependent. It is determined from kinematics at low incident energies. At higher energies the  $J_{\max}$  reaches a critical value  $J_{\text{cr}}$  and thereafter it remains constant.

## B. Comparison of calculated results with experimental data

In Fig. 4, we present the comparison of calculated results and experimental data for excitation functions in  $xn$  channels for the reactions  $^{40}\text{Ar} + ^{144}\text{Sm}$  and  $^{48}\text{Ca} + ^{142}\text{Nd}$ . One can see that the maxima of excitation functions for neutron-deficient CN  $^{184}\text{Hg}$  are lower than those for CN  $^{190}\text{Hg}$ . For example, in  $5n$  channel this difference is one order of magnitude. It is not only because of the difference in particle separation

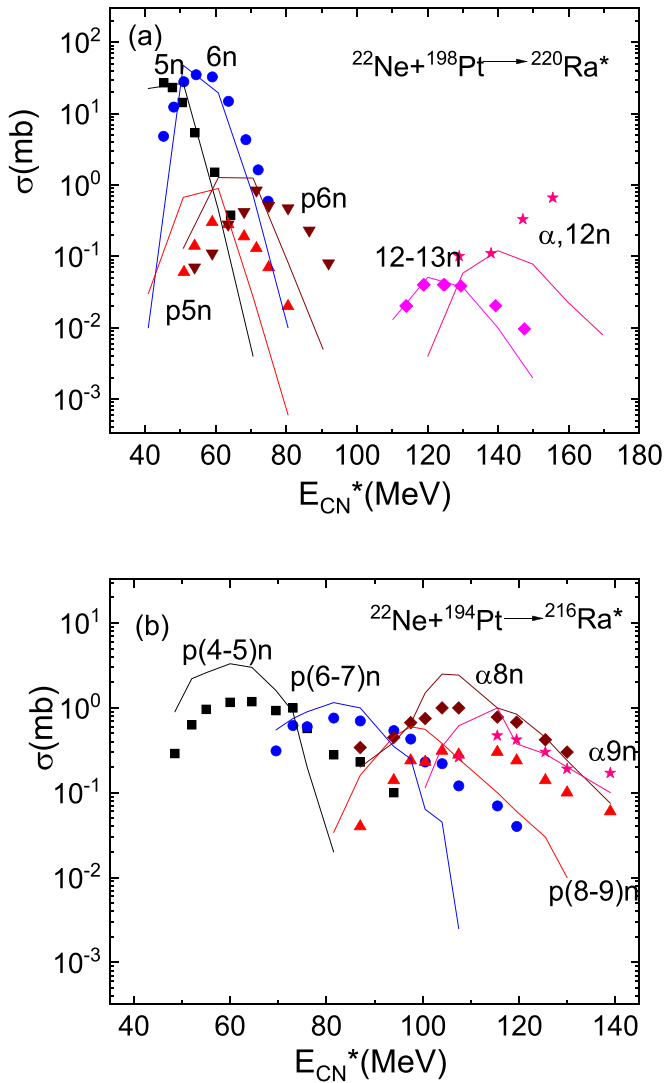


FIG. 10. Comparison of calculated (lines) and experimental (symbols) data for excitation functions in the (a)  $xn$  and (b)  $pxn$ ,  $\alpha xn$  evaporation channels of the reactions  $^{22}\text{Ne} + ^{198}\text{Pt}$  and  $^{22}\text{Ne} + ^{194}\text{Pt}$  leading to excited radium isotopes as the CN. The experimental data are taken from Ref. [22].

energies of these isotopes, but also because of higher formation probability of symmetric DNS in neutron-deficient CN  $^{184}\text{Hg}$  (see Fig. 1). This phenomenon leads to the increased yield of fissionlike fragments.

Similar behavior of excitation functions in  $xn$  channels with neutron deficiency is observed in the reactions leading to excited CN of polonium isotopes (Fig. 5). As found, the calculated maxima of excitation functions for  $4n$  (in the  $^{44}\text{Ca} + ^{160}\text{Gd}$  reaction) and  $3n$  (in the  $^{44}\text{Ca} + ^{156}\text{Gd}$  reaction) channels are shifted to higher energies comparing to the experimental ones because we consider  $E_{c.m.}$  larger than the height of the Coulomb barrier for spherical colliding nuclei, while smaller  $E_{c.m.}$  contribute to the experimental data as well. As seen in Table I, the excitation energy of CN at the Coulomb barrier is 46–50 MeV for these reactions, so the corresponding  $J_{max}$  values are very small. In Ref. [20], the ER were not

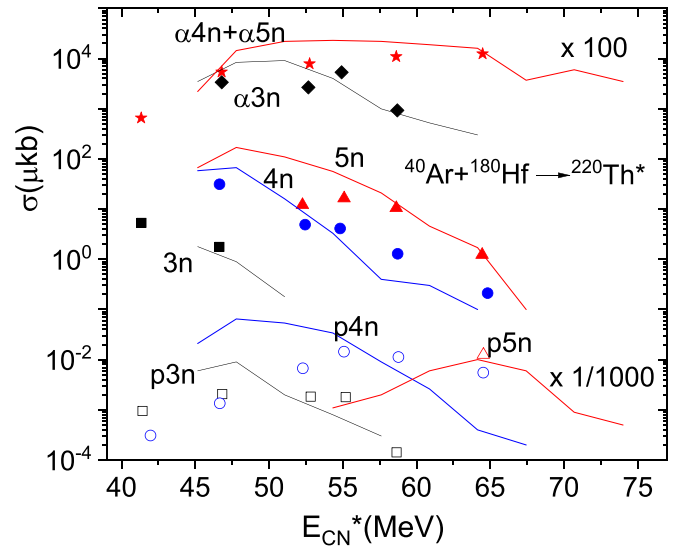


FIG. 11. Comparison of calculated (lines) and experimental (symbols) data for excitation functions in the  $xn$ ,  $pxn$ , and  $\alpha xn$  channels of the  $^{40}\text{Ar} + ^{180}\text{Hf} \rightarrow ^{220}\text{Th}^*$  reaction. The experimental data are taken from Ref. [23].

observed in the  $3n$  channel of the  $^{44}\text{Ca} + ^{160}\text{Gd}$  reaction due to the higher excitation energy of CN at the Coulomb barrier than it is required for  $3n$  channel. Calculated excitation functions in  $pxn$  and  $\alpha xn$  channels of the  $^{44}\text{Ca} + ^{160}\text{Gd}$  reaction are shown in Fig. 6. As seen in Figs. 5(a) and 6, for the excited CN  $^{204}\text{Po}$ , the maxima of excitation functions in  $xn$ ,  $pxn$ , and  $\alpha xn$  evaporation channels are rather comparable. This fact should be taken into account in analyzing the survival probabilities of the CN formed in these reactions. The extraction of fission barriers from the experimental  $\Gamma_f/\Gamma_n$  in these reactions will be inaccurate because of the enhanced emission of  $p$  and  $\alpha$  particles from neutron-deficient CN.

In Figs. 7–9, the excitation functions in  $xn$ ,  $pxn$ , and  $\alpha xn$  evaporation channels are presented for the fusion reactions resulting in different radon isotopes as the CN. Calculated excitation functions are in good agreement with experimental data. One can see again that maxima of excitation functions in  $xn$ ,  $pxn$ , and  $\alpha xn$  channels are comparable. Since with the neutron deficiency the binding energy of neutron increases, the cross sections in the  $xn$  channels decrease with increasing the number of emitted neutrons due to the growing competition with other decay channels.

In Figs. 10 and 11, the excitation functions in  $xn$ ,  $pxn$ , and  $\alpha xn$  evaporation channels are presented for the fusion reactions leading to excited isotopes of radium and thorium as the CN. As seen, the cross sections decrease by about two orders of magnitude in the  $^{40}\text{Ar} + ^{180}\text{Hf}$  reaction comparing to those in the  $^{48}\text{Ca} + ^{142}\text{Nd}$  and  $^{40}\text{Ar} + ^{144}\text{Sm}$  reactions. This result is explained by the driving potentials for these systems. The potential energy minimum at the symmetric DNS for thorium (Fig. 2) is deeper than those for Hg isotopes (Fig. 1). This leads to larger formation probabilities of symmetric DNS in the  $^{40}\text{Ar} + ^{180}\text{Hf}$  reaction than in the reactions  $^{48}\text{Ca} + ^{142}\text{Nd}$

and  $^{40}\text{Ar} + ^{144}\text{Sm}$ , which in turn leads to larger cross sections for fissionlike fragments in the  $^{40}\text{Ar} + ^{180}\text{Hf}$  reaction.

The neutron-deficient nuclei produced are almost spherical and can emit  $\alpha$  particles, with the exception of Pb and Bi isotopes, which can not be detected by  $\alpha$  decays. The properties of these nuclei are the subject of intensive study [24–27]. The probability of  $\alpha$  decay increases with decreasing mass number of isotope. Our calculations with the microscopic-macroscopic model [28] indicate that the ground-state spins of nuclei in the  $\alpha$ -decay chains  $^{215}\text{Ac} \rightarrow ^{211}\text{Fr} \rightarrow ^{207}\text{At}$ ,  $^{211}\text{Ac} \rightarrow ^{207}\text{Fr} \rightarrow ^{203}\text{At}$ , and  $^{207}\text{Ra} \rightarrow ^{203}\text{Rn} \rightarrow ^{199}\text{Po}$  are  $9/2^-$ ,  $9/2^-$ , and  $3/2^-$ , respectively, which agrees well with the experiment [29]. In the  $\alpha$ -decay chains, the  $\alpha$ -decay branching ratio decreases. For example,  $^{215}\text{Ac}$  and  $^{207}\text{At}$  go to  $\alpha$  decay with probabilities of 99.9% and 8.6%, respectively [29]. In the nuclei of  $\alpha$ -decay chain starting from  $^{207}\text{Ra}$ , there is low-lying isomeric state  $13/2^+$ . Thus, these nuclei can emit  $\alpha$  particles from both the ground state and the isomeric one. Note that for these nuclei the measured  $\alpha$ -decay half-lives are larger than 100 ms [26].

#### IV. SUMMARY

Based on the DNS approach, the proposed statistical model considers in a single way such reaction channels as particle emission, fusion-fission, and quasifission. The decay of

excited CN was treated through various DNS states. The excitation functions of ER in the  $xn$ ,  $pxn$ , and  $\alpha xn$  channels for the complete fusion reactions leading to CN with  $Z = 80$ –90 were investigated within this model. The cross sections for production of neutron-deficient nuclei  $^{179-185}\text{Hg}$ ,  $^{195-200}\text{Po}$ ,  $^{197-203}\text{At}$ ,  $^{198-200}\text{Bi}$ ,  $^{195-197}\text{Pb}$ ,  $^{201-204}\text{Rn}$ ,  $^{206-211}\text{Fr}$ ,  $^{211-215}\text{Ra}$ ,  $^{214-216}\text{Ac}$ , and  $^{215-217}\text{Th}$  were calculated. The theoretical results are in good agreement with the available experimental data for all reactions considered. Such type of reactions seem to be suitable for producing neutron-deficient isotopes with the cross sections larger than  $1 \mu\text{b}$ .

The results show that the maxima of excitation functions in the  $xn$ ,  $pxn$ , and  $\alpha xn$  channels are comparable for the reactions leading to compound nuclei from Hg to Th. This means that  $p$ - and  $\alpha$ -particle emission along with neutron emission influence the survival probability of CN in these reactions. Neutron deficiency of CN leads to favor both charged particle emission and fission. With increasing  $Z_{\text{CN}}$ , the probability of formation of symmetric DNS increases and the ratio of the probability of particle emission to the probability of fission decreases.

#### ACKNOWLEDGMENTS

We would like to thank Dr. A. Rahmatinejad for fruitful discussions in preparing the manuscript. This work was partly supported by the Ministry of Science and Higher Education of the Russian Federation (Contract No. 075-10-2020-117).

- 
- [1] Y. T. Oganessian, *J. Phys. G: Nucl. Part. Phys.* **34**, R165 (2007).
- [2] Y. T. Oganessian and V. K. Utyonkov, *Nucl. Phys. A* **944**, 62 (2015).
- [3] S. Hofmann, *J. Phys. G: Nucl. Part. Phys.* **42**, 114001 (2015).
- [4] G. Münzenberg, M. Gupta, H. M. Devaraja, Y. K. Gambhir, S. Heinz, and S. Hofmann, *Eur. Phys. J. A* **59**, 21 (2023).
- [5] M. S. Tezekbayeva, A. V. Yeregin, A. I. Svirikhin, A. Lopez-Martens, M. L. Chelnokov, V. I. Chepigin, A. V. Isaev, I. N. Izosimov, A. V. Karpov, A. A. Kuznetsova, O. N. Malyshev, R. S. Mukhin, A. G. Popeko, Y. A. Popov, V. A. Rachkov, B. S. Saïlaubekov, E. A. Sokol, K. Hauschild, H. Jacob, R. Chakma *et al.*, *Eur. Phys. J. A* **58**, 52 (2022).
- [6] M. La Commara, J. Gómez del Campo, A. D’Onofrio, A. Gadea, M. Glogowski, P. Jarillo-Herrero, N. Belcari, R. Borcea, G. de Angelis, C. Fahlander, M. Górska, H. Grawe, M. Hellström, R. Kirchner, M. Rejmund, V. Roca, E. Roeckl, M. Romano, K. Rykaczewski, K. Schmidt *et al.*, *Nucl. Phys. A* **669**, 43 (2000).
- [7] G. G. Adamian, N. V. Antonenko, A. Diaz-Torres, and S. Heinz, *Eur. Phys. J. A* **56**, 47 (2020).
- [8] G. G. Adamian, N. V. Antonenko, and W. Scheid, *Nucl. Phys. A* **618**, 176 (1997).
- [9] A. K. Nasirov, G. Giardina, G. Mandaglio, M. Manganaro, F. Hanappe, S. Heinz, S. Hofmann, A. I. Muminov, and W. Scheid, *Phys. Rev. C* **79**, 024606 (2009).
- [10] O. I. Davydovska, V. Y. Denisov, and I. Y. Sedykh, *Phys. Rev. C* **105**, 014620 (2022).
- [11] S. A. Kalandarov, G. G. Adamian, N. V. Antonenko, and W. Scheid, *Phys. Rev. C* **82**, 044603 (2010).
- [12] V. V. Volkov, G. G. Adamian, N. V. Antonenko, E. A. Cherepanov, and A. K. Nasirov, *Nuovo Cim. A* **110**, 1127 (1997).
- [13] G. G. Adamian, N. V. Antonenko, W. Scheid, and V. V. Volkov, *Nucl. Phys. A* **633**, 409 (1998).
- [14] G. G. Adamian, N. V. Antonenko, and W. Scheid, Clustering effects within the dinuclear model, *Clusters in Nuclei*, edited by C. Beck, Lecture Notes in Physics Vol. 848 (Springer, Berlin, Heidelberg, 2012), pp. 165–227.
- [15] G. G. Adamian and N. V. Antonenko, *Eur. Phys. J. A* **58**, 111 (2022).
- [16] I. S. Rogov, G. G. Adamian, and N. V. Antonenko, *Phys. Rev. C* **104**, 034618 (2021).
- [17] H. Pasca, A. V. Andreev, G. G. Adamian, and N. V. Antonenko, *Phys. Rev. C* **104**, 014604 (2021).
- [18] G. G. Adamian, N. V. Antonenko, and W. Scheid, *Phys. Rev. C* **68**, 034601 (2003).
- [19] D. Kamas, A. Opichal, E. V. Chernysheva, S. N. Dmitriev, A. V. Gulyaev, A. V. Gulyaeva, M. Holik, J. Kliman, A. B. Komarov, L. Krupa, A. S. Novoselov, Y. T. Oganessian, A. V. Podshibyakin, A. M. Rodin, V. S. Salamatin, S. V. Stepantsov, V. Y. Vedenev, and S. A. Yuhimchuk, *Phys. Rev. C* **105**, 044612 (2022).
- [20] T. A. Werke, C. S. Salas, K. J. Glennon, D. A. Mayorov, E. E. Tereshatov, M. F. Volia, D. M. Wright, and C. M. Folden, *Phys. Rev. C* **106**, 054615 (2022).
- [21] A. N. Andreyev, D. D. Bogdanov, V. I. Chepigin, A. P. Kabachenko, O. N. Malyshev, Y. T. Oganessian, A. G. Popeko,

- J. Roháč, R. N. Sagaidak, G. M. Ter-Akopian, A. V. Yeremin, Š. Šáro, and M. Veselský, *Nucl. Phys. A* **626**, 857 (1997).
- [22] A. N. Andreyev, D. D. Bogdanov, V. I. Chepigin, A. P. Kabachenko, O. N. Malyshev, Y. A. Muzichka, Y. T. Oganessian, A. G. Popeko, B. I. Pustyl'nik, R. N. Sagaidak, G. M. Ter-Akopian, and A. V. Yeremin, *Nucl. Phys. A* **620**, 229 (1997).
- [23] C. C. Sahm, H. G. Clerc, K. H. Schmidt, W. Reisdorf, P. Armbruster, F. P. Hessberger, J. G. Keller, G. Münzenberg, and D. Vermeulen, *Nucl. Phys. A* **441**, 316 (1985).
- [24] P. Hornshøj, K. Wilsky, P. G. Hansen, A. Lindahl, O. B. Nielsen, and the ISOLDE collaboration, *Nucl. Phys. A* **163**, 277 (1971).
- [25] J. Wauters, K. Dendooven, M. Huyse, G. Reusen, P. Van Duppen, L. Lievens, and the ISOLDE collaboration, *Phys. Rev. C* **47**, 1447 (1993).
- [26] F. P. Heßberger, S. Hofmann, D. Ackermann, V. Nilov, M. Leino, S. Saro, A. Andreyev, A. Lavrentev, A. G. Popeko, and A. V. Yeremin, *Eur. Phys. J. A* **8**, 521 (2000).
- [27] E. Caurier, M. Rejmund, and H. Grawe, *Phys. Rev. C* **67**, 054310 (2003).
- [28] G. G. Adamian, L. Malov, N. V. Antonenko, H. Lenske, K. Wang, and S.-G. Zhou, *Eur. Phys. J. A* **54**, 170 (2018).
- [29] National Nuclear Data Center (nndc), <http://www.nndc.bnl.gov> (2023).